The Effects of Different Gas Models on the Hypersonic Viscous Flow over Reentry Vehicles

Shen Jianwei Qu Zhanghua

Department of Astronautical Engineering
Changsha Institute of Technology
Changsha, Hunan, P.R. China

Abstract

In this paper, the hypersonic viscous flow over reentry vehicle with different gas models is analyzed numerically. The multi-component ionizing air, ideal dissociating oxygen and perfect gas are considered. The viscous shock-layer equations are used for describing the flowfield, and they are solved in space-marching technique with implicit finite-difference scheme. Seven species (N_2, O_2, N, O, NO, NO^+, e^-) as well as seven chemical reactions are considered for the multi-component air. The chemical reactions are assumed to procced at finite rate.

The numerical results show that the specific heat ratio in hypersonic flowfield is no longer a constant, and the average value is less than 1.4. The concept of equivalent specific heat ratio will improve some of the difference between perfect gas and reacting gas, but the surface heat transfer is an exception. As the chemical reactions take place at high temperature, the transport properties of the air will differ from Suthertand's law, and it is necessary to consider the real-gas effects.

Nomenclature

C_i	concentration of species i
C_p	specific heat at constant pressure
C_{p_i}	specific heat of species i
$g(\eta)$	grid stretching function
h	static enthalpy
k_i	thermal conductivity of species i
k	thermal conductivity of mixture
K_{br}	backward rate constant
K_{fr}	forward rate constant
M_∞	Mach number
M_i	molecular weight of species i
$\bar{M}$	average molecular weight of mixture $\bar{M}=1/(\sum_i \frac{C_i}{M_i})$
n	coordinate measured normal to the body surface, n^*/R_n^*
ns	number of species
n_{sh}	shock standoff distance
P	non-dimensional pressure, $P^*_\infty/(\rho^*_\infty U^{*2}_\infty)$
Pr	Prandtl number
Qw	heat transfer rate at the wall, $Q_w^*/(\rho^*_\infty U^{*3}_\infty)$
R_n	nose radius
s	coordinate measured along the body surface, s^*/R_n^*
U_∞	velocity of free stream
α_{ri}	stoichiometric coefficients for reactions
β_{ri}	stoichiometric coefficients for reactions
γ	specific heat ratio
ϵ	Reynolds number parameter, $\epsilon=[\mu^*_{ref}/(\rho^*_\infty U^*_\infty R_n^*)]^{1/2}$
ξ, η	normalized coordinates
μ_i	viscosity of species i
μ	viscosity of mixture
ρ	density, ρ^*/ρ^*_∞

Subscripts

∞	free stream condition
ref	reference condition

Superscript

*	dimensional properties

Introduction

As the hypersonic vehicles reenter into the atmosphere, the air in the viscous shock-layer may be dissociated and ionized at high temperature, the specific heat ratio of the air is no longer a constant, and the shock shape, as well as surface pressure distribution may be different from the results of perfect gas model. It is necessary to consider the real-gas effects for the hypersonic reentry vehicles.

At the high altitude, the air density and Reynolds number are so low that the ordinary boundary equations are no longer adequate, but the full viscous shock-layer equations can be used for describing the flowfield. The viscous shock-layer equations contain the second order terms of the Reynolds number parameter ϵ of the Navier-Stokes equations, which is higher in accuracy than that of the boundary equations. The uniform equations are used in both the viscous and invisid flow regions, which avoid the trouble

caused by the interaction between the viscous and invisid layers. The viscous shock-layer equations are mainly hyperbolic and parabolic, the elliptic effects of unknown shock shape may be overcome through global iteration. The equations can be solved in space-marching technique[3]. As the nonequilibrium chemical reactions among the components of the air are considered, the species conservation equations are added in governing equations, and the relevant heat formation terms are appear in the energy equation.

In this paper, the effects of three different gas models on the properties of hypersonic flowfield are analyzed with viscous shock-layer equations. Seven species reacting air, ideal-dissociating oxygen and perfect gas models are considered, the results of different gas models are compared.

Analysis

Governing Equations and Boundary Conditions

The chemical nonequilibrium viscous shock-layer equations and boundary conditions in body oriented coordinats are given in reference[12]. For the perfect gas model, the species conservation equations and the relevant heat formation term in the energy equation are eliminated, the momentum equations and global continuity equation are the same as reacting gas model.

Transport Properties and Chemical Reacting Model

For the reacting gas, the enthalpy and specific heat of the species are got from the datalist given by Browne[6] [7]. The enthalpy and specific heat of the mixture gas are calculated as follows,

$$h = \sum_{i=1}^{ns} h_i C_i$$

$$Cp = \sum_{i=1}^{ns} Cp_i C_i$$

The viscosity of species is given by curve fit relations,

$$\mu_i = \exp(C_i) T_k^{(A_i \ln T_k + B_i)}$$

where A_i, B_i and C_i are different constants taken from Blottner[8], T_k is local temperature.

Species heat conductivity is calculated as follows,

$$k_i = \frac{\mu_i}{M_i} R \left(\frac{Cp_i M_i}{R} + \frac{5}{4} \right)$$

where M_i is molecular weight of species i. the viscosity and heat conductivity of the mixture are calculated by,

$$\mu = \sum_{i=1}^{ns} \frac{X_i \mu_i}{\sum_{j=1}^{ns} X_j \Phi_{ij}}$$

$$k = \sum_{i=1}^{ns} \frac{X_i k_i}{\sum_{j=1}^{ns} X_j \Phi_{ij}}$$

where

$$X_i = C_i \frac{\bar{M}}{M_i}$$

$$\Phi_{ij} = \left[1+(\mu_i/\mu_j)^{1/2}(M_j/M_i)^{1/4}\right]^2 \Big/ \left[8(1+M_i/M_j)\right]^{1/2}$$

$\bar{M}$ is the average molecular weight of the mixture.

For the perfect gas model, the specific heat ratio γ is taken as a constant. The viscosity is calculated by Sutherland's law as follows,

$$\mu = \frac{1 + C}{T + C} T^{3/2}$$

where

$$C = 110.3 / [(\gamma - 1) M_\infty^2 T_\infty]$$

The thermal conductivity is calculated by

$$k = \frac{\mu Cp}{Pr}$$

For the chemical nonequilibrium reacting gas, seven species are considered, N2, O2, N, O, NO, NO^+, e^-, the chemical reactions among them are as follows,

$$O2 + M1 \rightleftharpoons 2O + M1$$
$$N2 + M2 \rightleftharpoons 2N + M2$$
$$N2 + N \rightleftharpoons 2N + N$$
$$NO + M3 \rightleftharpoons N + O + M3$$
$$NO + O \rightleftharpoons O2 + N$$
$$N2 + O \rightleftharpoons NO + N$$
$$N + O \rightleftharpoons NO^+ + e-$$

where M1, M2, M3 are third catalytic bodies.

The forward and backward reacting cons-

tants K_{fr}, K_{br} are taken from Blottner[8] for determining the species formation terms.

For the ideal dissociating oxygen, it is assumed that the air is composed of oxygen moleculars and atoms.

Numerical Calculation

In numerical calculation, the following coordinate transformations are used,

$$\bar{\xi} = s \tag{1}$$

$$\bar{\eta} = \frac{n}{n_{sh}(\bar{\xi})}$$

$$\xi = \bar{\xi} \tag{2}$$

$$\eta = g(\bar{\eta})$$

where

$$g(\bar{\eta}) = 1 - \alpha - \frac{1-\alpha}{\ln\left(\frac{\beta+1}{\beta-1}\right)} \ln\left(\frac{\beta - \bar{\eta}(2\alpha+1)+1}{\beta + \bar{\eta}(2\alpha+1)-1}\right)$$

β is the coefficent of the grid stretch, α is alternative parameter, $\alpha=0$, the grids are only stretched near the body surface, $\alpha=1/2$, the grids are stretched both near the bow shock and the body surface.

The flowfield from the body surface to bow shock become a regular region through transformation (1), thus the square grids can be used. Transformation (2) is used for adding more grids near the shock and body surface as the total grids do not change, so that it is adequate for large gradient of the flowfield properties.

The physical properties of the flowfield are normalized by the values at bow shock with the exception of the normal velocity and species concentrations to avoid taking zero as denominator.

Numerical calculation started from the stagnation line, then marching downstream along the body surface. On the stagnation line, the physical properties and geometric parameters are expanded as a series of ξ, so that the governing equations become a set of ordinary differential equations, and they are solved with finite-difference method. The solutions of stagnation line are used as the initial value of space marching.

The tangential momentum equation, energy equation and species continuity equation can be expressed as standard parabolic equation, and they are solved with Stoimachic algorithm. As the energy equation and species equations are written in the standard parabolic form, the formation terms are disposed for the quasi-linearization. The global continuity conservation equation and normal momentum equation are solved in a coupled way[11], which greatly improved the convergency. The shock standoff distance is determined by integration of the global continuity equation.

The implicit-finite difference method are used in the numerical calculation for its good stability, and a suitable large space marching step size can be used, but only one order of accuracy is maintained in s direction, hence the schematic viscousity may be included in the difference equation. From the analysis of reference[12], it can be known that the effects of schematic viscosity is not serious.

Results and Discussion

The hypersonic viscous shock-layer flow over reentry blunt bodies are numerically calculated. The velocity of freestream flow is 7.6 km/s, body surface temperature is 1000° K, hyperboloid with half angle 9° is considered, angle of attack is zero. Fig.1 is the distribution of specific heat ratio of reacting gas model, the altitude are 75 km, 85 km and 92 km respectively. The results show that the specific heat ratio of reacting gas is less than 1.4, and the average value is about 1.3. At the nose region, the temperature at the bow shock is about two order of magnitude higher than that of the free stream flow, and the high temperature caused the gas to excite, and the specific heat ratio Cp/Cv is reduced. For the binary gas model, all the oxygen moleculars almost dissociated into monoatomic gas, so that the specific heat ratio may reach 1.6, (i.e. it approximates to the monoatomic specific heat ratio 5/3), At the far downstream region, the shock is oblique, and the dissociation degree of air is reduced, so that γ is near 1.3. The results also show that the specific heat ratio reduces as the altitude is raised. This is because at higher altitute, the low density reduces the degree of dissociation, then the effects of single atoms are small, so that the specific heat ratio is reduced.

Fig.2 is the results of shock stand-off distance for different gas model. The results show that the value of perfect gas ($\gamma=1.4$) is larger than that of reacting gas, As the specific heat ratio is taken larger, it effects the gas density through the state equation, and made the shock stand-off distance larger. As γ is taken the value of 1.3, the difference between perfect gas and reacting gas is appearently improved.

Fig.3 is the comparison of surface pressure distribution. At the nose region, the shock shape is near normal shock, the shock layer is thicker for perfect gas,

then the density ratio and pressure ratio are smaller, so that the surface pressure of perfect gas is lower than that of reacting gas. in the far downsteam region, a large γ made the shock shape expand, and the shock angle is bigger, hence the surface pressure of pefect gas is larger than that of reacting gas. This kind of difference of surface pressure distribution between nose region and downstream region may make the lift force of space shuttle differ from the theoritical value of perfect gas model.

Fig.4 is the results of surface heat transfer distribution. As the chemical reactions are considered, the surface heat transfer is less than that of perfect gas. This is because the chemical reactions must absorb some of the heat. The heat transfer of binary gas model is near the value of seven species reacting mixture. In fact, the dissociation of binary molecular represents the major reactions of the air. The results show that as γ is taken the value of 1.3, the heat transfer is differ more from reacting gas model, which indicates that the concept of equivalent specific heat ratio is not proper for the surface heat transfer.

Fig.5 and Fig.6 are the results of viscosity and thermal conductivity respectively In the nose region, the difference between the Sutherland's law and curve fit is about 30%, at the downstream region, the difference is about 10%. Those results show that it is necessary to consider the real-gas effects for the transport properties of the chemical reacting gas.

As shown by the comparison in Fig.7, our solution is fairly close to the Cleary's[13].

Concluding Remark

From the analysis of this study, it can be known that the specific heat ratio is less than 1.4 for hypersonic flow, and it is no longer an important parameter for reacting gas. The binary species reacting gas model is applied to a simple method, which greatly reduced the computer time, and the results are near that of the multi-component gas model, but it can not get the electron number density distribution. As γ is taken the value of 1.3 for perfect gas, surface pressure distribution and shock standoff distance are improved as compared with reacting gas, but surface heat transfer is more different from the reacting gas. As the nonequilibrium chemical reactions are considered, it is adequate using curve fit to calculate the transport properties of the mixture.

Acknowledgment

The authors are thankful to Chinese Natural Science Fund Committee for the financial support of this study.

References

1. Gupta, R.N., Lee, K.P., Moss, J.N., Zoby, E.V. and Tiwari, S.N., Viscous Shock-Layer Analysis of Hypersonic Flows over Long Slender Bodies, AIAA Paper No.87-2487, 1987.
2. Swaminathan, S., Kim, M.D. and Lewis, C.H., Nonequilibrium Viscous Shock-Layer Flow over Blunt Sphere-Cones at Angle-of-Attack, AIAA Paper No.82-0825, 1982.
3. Davis, R.T., Numerical Solution of the Hypersonic Viscous Shock Layer Equations, AIAA Journal, Vol.8, No.5, May 1970, pp.843-851.
4. Moss, J.N., Reacting Viscous-Shock-Layer Solutions with Multicomponent Diffusion and Mass Injection, NASA TR R-411, June 1974.
5. Miner, E.W. and Lewis, C.H., Hypersonic Ionizing Air Viscous Shock-Layer Flow over Nonanalytic Blunt Bodies, NASA CR-2550, May 1975.
6. Browne, W.G., Thermodynamic properties of some Diatoms and Diatomic Ions at High Temperature, MSD Adevanced Aerospace Physics TM8, General Electric Co., Philadelphia, Pa., May 1962.
7. Browne, W.G., Thermodynamic Properties of Some Atoms and Atomic Ions, MSD Engineering Physics TM2, General Electric Co. Philadelphia, Pa., 1962.
8. Blottner, F.G., Johnson, Margaret and Ellis, Molly, Chemically Reacting Viscous Flow Program for Multi-Component Gas Mixtures, Sandia Laboratories Report SC-RR-70-754, Dec.1971.
9. Cheng, H.K., The Blunt-Body Problem in Hypersonic Flow at Low Reynolds Number, IAS Paper No.63-92, Jan. 1963.
10. Shen Jianwei and Qu Zhanghua, Ionized Nonequilibrium Viscous Shock-Layer Flows over Blunt Bodies at Low Reynolds. ACTA AERODYNAMICA SINICA, Vol.4, No.4, 1986.
11. Shen Jianwei and Qu Zhanghua, Numerical Calculation of Hypersonic Nonequilibrium Viscous Shock-Layer Flow over a Slender Body with Blunt Nose, Journal of Chinese Society of Astronautics, No.3, 1988.
12. Shen Jianwei, Numerical Solution of the Hypersonic Viscous Shock-Layer Equations with Chemical Non-equilibrium, IAF-ST-8808, Oct. 1988.
13. Cleary, J.W., Effects of Angle of Attack and Bluntness on Laminar Heating-Rate Distributions of a 15 Deg. Cone at a Mach Number of 10.6, NASA TN D-5450, 1969.
14. Randolph A.Graves, Jr. and James L. Hunt, NASA's Hypersonic Fluid and Thermal Physics Program (Aerothermadynamics), AIAA Paper No. 85-0992, 1985.

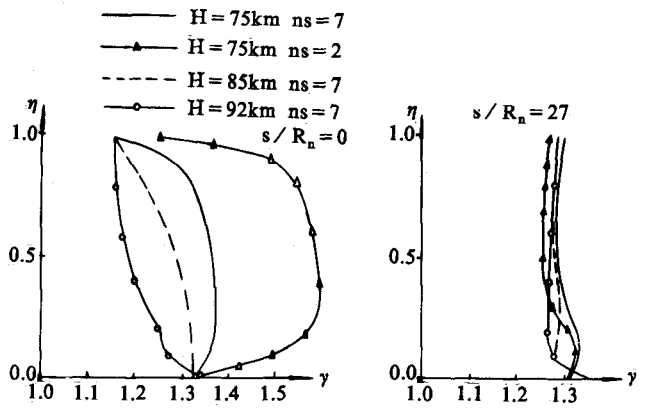

Fig. 1 Specific heat ratio of reacting gas

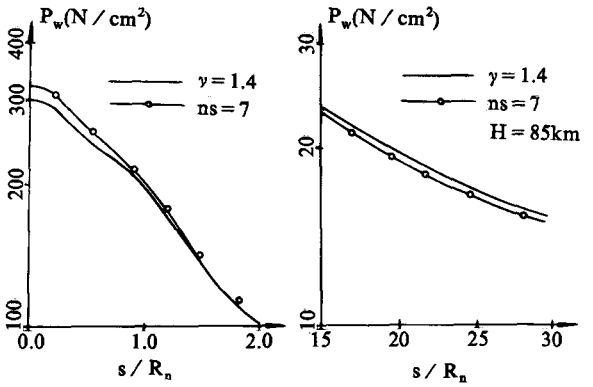

Fig. 3a Surface pressure distribution

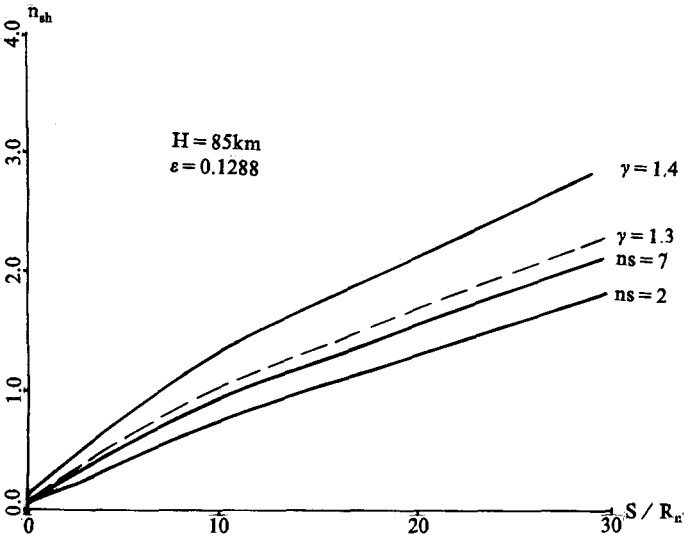

Fig. 2 Shock stand-off distance

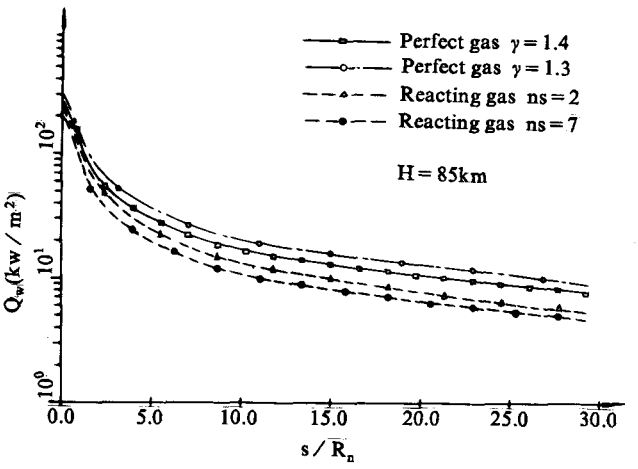

Fig. 4 Surface heat transfer distribution

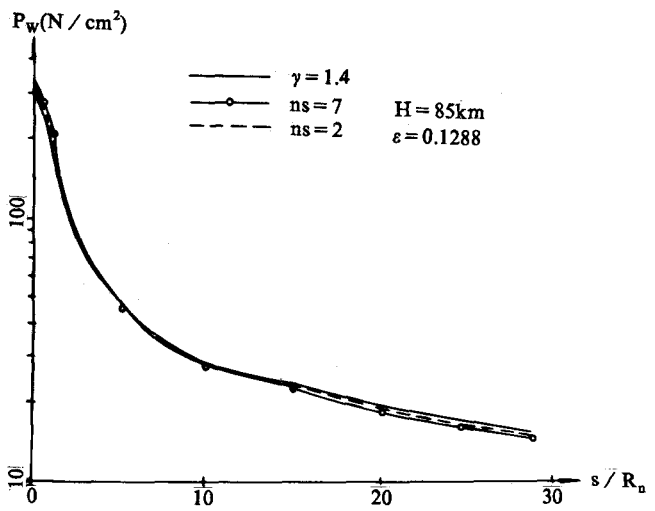

Fig. 3 Surface pressure distribution

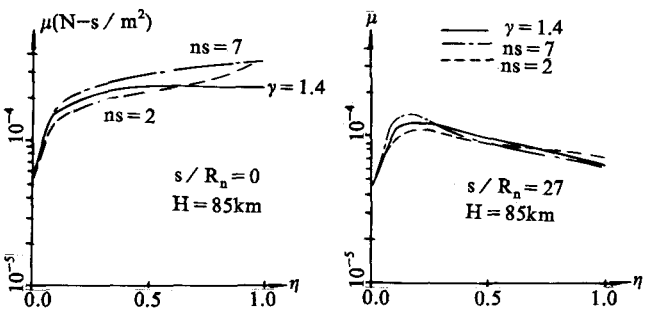

Fig. 5 Comparison of viscosity distribution

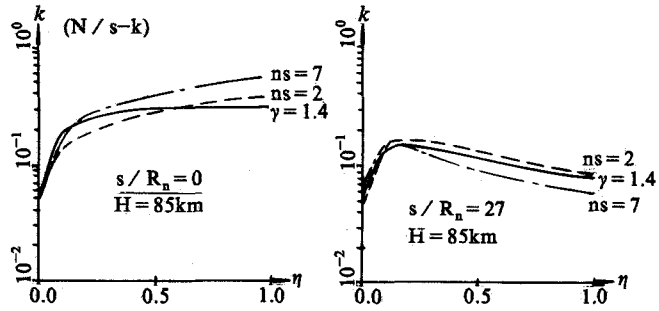

Fig.6 Comparison of conductivity distribution

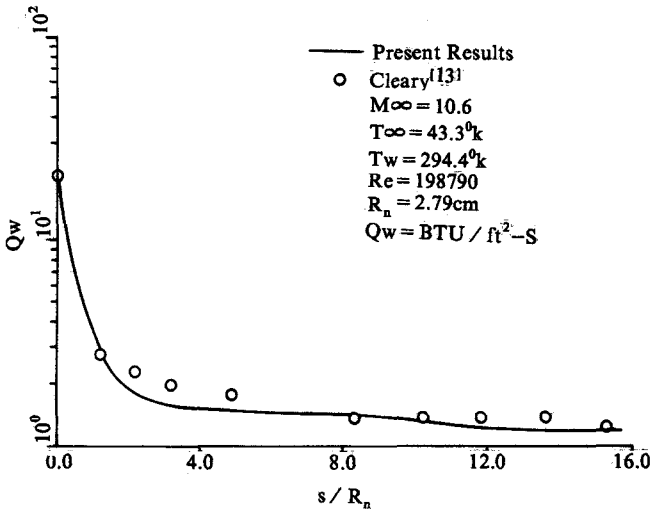

Fig.7 Comparison of surface heat transfer